

Article

PCL and DMSO₂ Composites for Bio-Scaffold Materials

Jae-Won Jang ¹, Kyung-Eun Min ¹, Cheolhee Kim ^{1,2} , Chien Wern ¹  and Sung Yi ^{1,*}¹ Department of Mechanical and Material Engineering, Portland State University, Portland, OR 97201, USA² Welding and Joining R&D Group, Korea Institute of Industrial Technology, 156, Getbeol-ro, Yeonsu-gu, Incheon 21999, Republic of Korea

* Correspondence: syi@pdx.edu

Abstract: Polycaprolactone (PCL) has been one of the most popular biomaterials in tissue engineering due to its relatively low melting temperature, excellent thermal stability, and cost-effectiveness. However, its low cell attraction, low elastic modulus, and long-term degradation time have limited its application in a wide range of scaffold studies. Dimethyl sulfone (DMSO₂) is a stable and non-hazardous organosulfur compound with low viscosity and high surface tension. PCL and DMSO₂ composites may overcome the limitations of PCL as a biomaterial and tailor the properties of biocomposites. In this study, PCL and DMSO₂ composites were investigated as a new bio-scaffold material to increase hydrophilicity and mechanical properties and tailor degradation properties in vitro. PCL and DMSO₂ were physically mixed with 10, 20, and 30 wt% of DMSO₂ to evaluate thermal, hydrophilicity, mechanical, and degradation properties of the composites. The water contact angle of the composites for hydrophilicity decreased by 15.5% compared to pure PCL. The experimental results showed that the mechanical and degradation properties of PCL and DMSO₂ were better than those of pure PCL, and the properties can be tuned by regulating DMSO₂ concentration in the PCL matrix. The elastic modulus of the composite with 30 wt% of DMSO₂ showed 532 MPa, and its degradation time was 18 times faster than that of PCL.

Keywords: biomaterial; scaffold; additive manufacturing; material property; property tailoring

Citation: Jang, J.-W.; Min, K.-E.; Kim, C.; Wern, C.; Yi, S. PCL and DMSO₂ Composites for Bio-Scaffold Materials. *Materials* **2023**, *16*, 2481. <https://doi.org/10.3390/ma16062481>

Academic Editor: Agata Przekora-Kuśmierz

Received: 30 December 2022

Revised: 8 March 2023

Accepted: 18 March 2023

Published: 21 March 2023



Copyright: © 2023 by the authors. Licensee MDPI, Basel, Switzerland. This article is an open access article distributed under the terms and conditions of the Creative Commons Attribution (CC BY) license (<https://creativecommons.org/licenses/by/4.0/>).

1. Introduction

The goal of bone tissue engineering (BTE) is to regenerate or replace damaged bone [1–3]. Bone has a self-healing ability, but in critical-sized damage cases, bone tissue cannot be healed itself completely [4,5]. Therefore, external treatment is required in the latter case including autografts and allografts [6–8]. Although allograft is a main practice for repairing damaged bone tissues, a shortage of donors has still remained [9–11]. According to Health Resources & Services Administration (HRSA) data, over one hundred thousand people are on the national transplant waiting list, but only 40,000 transplants were performed in 2021 [12].

Porous scaffold, which mimics extracellular matrix (ECM), is a crucial technology for bone tissue engineering for cell attachment, proliferation, and supporting the human body [13]. ECM is a three-dimensional structure providing structural and biochemical support to surrounding cells in vivo [14]. Scaffold should have biocompatibility, biodegradability, and proper mechanical properties [15–17]. Moreover, geometry properties, fabrication methods, and biomaterials are also considered for scaffold manufacturing [18–20].

Scaffold materials can be divided into four groups: natural and synthetic polymers, bio-ceramics, metallic materials, and composites [21,22]. The synthetic polymer group is the most interesting material group because this group showed tunable mechanical and biodegradable properties as well as cost effect [23–25]. Polycaprolactone (PCL) is one of the famous synthetic bio-degradable polymers along with polylactic acid (PLA) and polyglycolide (PGA) [26]. PCL is already approved by Food and Drug Administration (FDA) as a biomaterial [27], and it has a relatively low melting temperature and excellent

thermal stability [28] as well as a cheap price [29]. PCL, however, has a very slow degradation time, and low cell attractive property because of its hydrophobic [30]. Moreover, relatively high viscosity of PCL needs high pressure when it is printed and it makes it hard to print accurately [31]. In spite of these disadvantages, PCL is widely used in various tissue engineering applications due to its attractive properties as mentioned above. Many of PCL-based composites are reported to overcome PCL's disadvantages [26].

Dimethyl sulfone (DMSO₂), known as Methylsulfonylmethane (MSM), is an organosulfur compound occurred naturally [32]. DMSO₂ is well known as an extremely stable and non-hazardous material, and it uses its unique properties to alter physiology at both the cellular and tissue levels [33]. DMSO₂ can also act as a carrier or co-transporter for other therapeutic agents, further expanding its applications [34]. Moreover, DMSO₂ can play a role in cartilage preservation [35]. There has long been a belief that cartilage degradation is one of the main reasons of osteoarthritis [36]. Articular cartilage is presented by a dense ECM and extracts nutrients from the adjacent synovial fluid with little to no blood [37]. In vitro studies indicate that DMSO₂ can protect cartilage [38], and it possibly normalizes hypoxia-driven alterations to cellular metabolism [39]. DMSO₂ has a low viscosity [40] that affects printing accuracy and high surface tension [41] which can improve hydrophilicity then can increase cell attractive property as a composite material in the biomaterial matrix [42].

A number of studies have attempted to improve the biomaterial properties of PCL-based scaffolds by conducting research on PCL-based composites [43–46]. PCL showed the slowest degradation time among polyester group polymers [15,47]. Fully degraded time of PCL was noted for about 2–3 years. PCL and 20 wt% of tricalcium phosphate (TCP) were fully degraded after 54 h even though the PCL scaffold took 6 weeks to entirely degrade in the accelerated degradation studies using 5 M sodium hydroxide (NaOH). Fifteen wt% of nano-hydroxyapatite (HA) decreased water contact angle of PCL from 112.98–79.50° [48]. Cellulose nanocomposites (CNC) were used to increase the elastic modulus of PCL-based composites [49]. However, there have not been enough studies of PCL-based composites to apply bone tissue engineering.

In this study, PCL and DMSO₂ composites were investigated as a new bio-scaffold material to increase the hydrophilicity and mechanical properties, and to tailor the degradation property in vitro. In detail, the tailored properties of PCL by mixing DMSO₂ with 10, 20, and 30 wt% of DMSO₂ were studied. Material properties including thermal, hydrophilicity, mechanical, and degradation properties of composites were measured. Hydrophilicity and modulus of composites were increased with the concentration of DMSO₂ in the PCL matrix, and degradation time was accelerated 1.2–18 times more than the pure PCL by DMSO₂ ratio. By regulating DMSO₂ concentrations, the properties of composites can be tailored to the specific situation.

2. Experiments

2.1. Materials

In this study, polycaprolactone (PCL) and PCL based composites with dimethyl sulfone (DMSO₂) were used for hydrophilicity, mechanical properties, and degradation time. Powder type PCL with a molecular weight 50,000 was provided from Polysciences (Warrington, PA, United States), and powder type DMSO₂ was provided from Bergstrom Nutrition (Vancouver, WA, United States). Both material properties provided by the manufacturer are shown in Table 1. In the pre-test of a composites, over 40 wt% of DMSO₂ were either too hard or brittle, resulting in them unsuitable for experiments. Composites were physically mixed with DMSO₂ concentrations of 10, 20, and 30 wt% using an electric milling machine (YUESUO, Zhengzhou, China). All materials were dried at 45 °C under vacuum condition for one day before mixing. In this paper, the composites were denoted by PCL/D10, PCL/D20, and PCL/D30 according to the DMSO₂ weight percent.

Table 1. Material properties of PCL and DMSO₂ provided by the manufacturer.

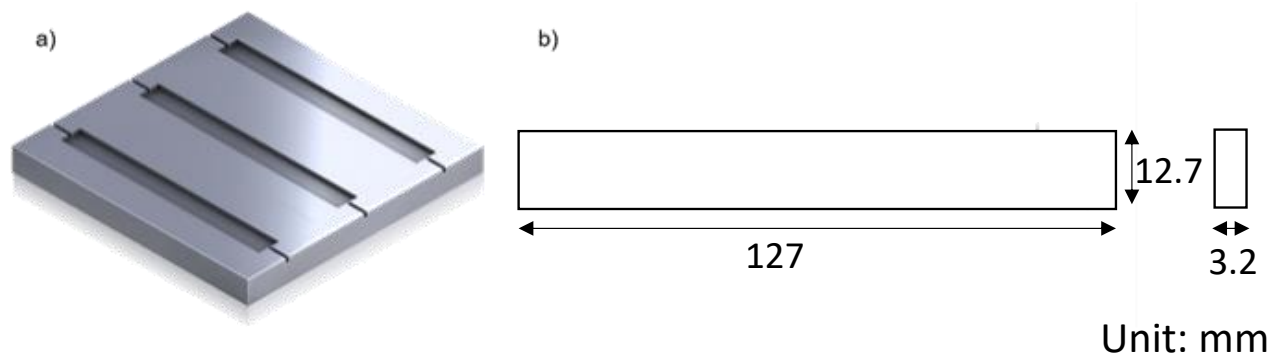
Material	Appearance	Molecular Weight (g/mol)	Density (kg/m ³)	Flash Point (°C)	Surface Tension (mN/m)	Viscosity (mPa·s)
PCL	Powder	50,000		275		
DMSO ₂	Powder	94.13	1450	143	60.15	1.14

2.2. Melting Temperature

The specimens for hydrophilicity, mechanical properties, and degradation test were fabricated by mold casting and additive manufacturing. A dynamic differential scanning calorimetry (DSC) method was performed to set a melting and a 3D printing temperature with heating and cooling rate of 5 °C/min. The temperature range of the test was 30–150 °C. The equipment was STA 8000 (PerkinElmer, Waltham, MA, United States) having a heat-flux type DSC with balance resolution of 0.2 µg and the temperature accuracy of ±0.5 °C from ambient to 1000 °C. The heating rate was determined by considering the 3D printer heating speed and the cooling rate was set the same as the heating rate. The melting temperature was set at the onset temperature under endothermic process [50,51].

2.3. Hydrophilicity

Specimens for hydrophilicity were fabricated by mold casting, and the target specimen size was 12.7 mm × 25.4 mm × 3.2 mm. The mold was designed according to the ASTM D790 standard [52] for the three-point bending test having 3 cavities of 127 mm × 25.4 mm × 3.2 mm (Figure 1). The solid material of pure PCL and mixed PCL and DMSO₂ composites were put into the mold, and the mold was placed on a hot plate heated 120 °C. The mold with fully melted materials was cooled at room temperature for 2 h, and the top surface of melted materials was flattened by a metal plate having a smooth surface during solidification. Casted bar was cut into 5 pieces for the test.

**Figure 1.** Mold design (a) and specimen sizes (b) for the mechanical test.

Hydrophilicity can be evaluated using contact angle by the sessile drop method according to the ASTM D7334 standard [53]. A common test liquid of hydrophilicity is distilled (DI) water. In this test, DI water and phosphate-buffered saline (PBS) solution were used as a test liquid. The test liquid of 10 µL was dropped to the specimen and the angle between the test liquid and the specimen was measured at the endpoints of the left and right. The test was performed 5 times and the contact angle was denoted by an average value.

2.4. Mechanical Test and Failure Analysis

Mechanical test specimens were fabricated by mold casting. The mold was the same used in the hydrophilicity test. The test specimen sizes were 12.7 mm × 127 mm × 3.2 mm.

The specimen manufacturing process was the same as the hydrophilicity test except for the cutting process.

Elastic modulus and 0.2% offset yield strength were measured by using the three-point bending test to evaluate the mechanical properties of the specimens. A bench-mounted universal testing machine of model 5ST (Tinius Olsen, Redhill, United Kingdom) was used for the test. The equipment has a maximum force of 5000 N with 0.2% load measuring accuracy of the reading 0.2–100% of the load cell capacity. The test was performed to the strain limit of 5%, and the test ended when the deflection of midspan of the materials reached to 6.8 mm. The rate of crosshead motion and the end condition of the test were calculated according to the ASTM D790 standard [52]. The test was performed using 5 samples, and the maximum and the minimum value were excepted when the mechanical properties were calculated.

The stress and the strain were calculated by

$$\sigma = \frac{3PL}{2bd^2} \quad (1)$$

$$\varepsilon = \frac{3Dd}{L^2} \quad (2)$$

where σ and ε are stress in the outer fibers at midpoint and strain in the outer surface, respectively. P is the load at a given point on the load-deflection curve, L is a support span, b is the width of tested beam, d is a thickness of tested beam and D is the maximum deflection of the center. Modulus in elasticity were obtained by load-deflection curve from above equations. Modulus in elasticity was calculated by

$$E = \frac{L^3m}{3bd^3} \quad (3)$$

where E is modulus in elasticity (MPa), and m is the gradient of the tangent to the initial straight-line portion of the load-deflection curve (N/mm).

In order to investigate the surface of the composites and the fracture surface after the test, a scanning electron microscope (SEM) analysis was performed. SNE-4500M Plus (SEC Co., Ltd., Suwon, Republic of Korea) was used. The surfaces of composites were coated with Au for 4 min using an ion sputter coater (MCM-100P, SEC Co., Ltd., Republic of Korea) before SEM analysis.

2.5. Degradation Test

Degradation test specimens were fabricated by the material extrusion process using Biobot (current model: Allevi2, Allevi, Inc., Philadelphia, PA, United States), a desktop pneumatic Extrusion 3D bioprinter. This equipment can control pressure and temperature with ranges of 6.895–827.371 kPa and from room temperature to 160 °C, respectively. The specimen shape was a cylindrical scaffold with a diameter of 14 mm and 20 layered, and each layer has a 360 μm (Figure 2). The target porosity of the scaffold was 55–58% under the above printing conditions. The porosity of the scaffold was measured by the printed scaffold weight. Original scaffold structure was designed using SOLIDWORKS 2021 (Dassault Systèmes, Vélizy-Villacoublay, France), and then sliced using Slic3r software version 1.2.9. To achieve the same surface area for all specimens, printing temperature and pressure were varied from 120 °C to 130 °C and from 30 psi to 70 psi, individually, but the printing speed and the nozzle inner diameter were fixed at 0.8 mm/s and 450 μm , respectively.

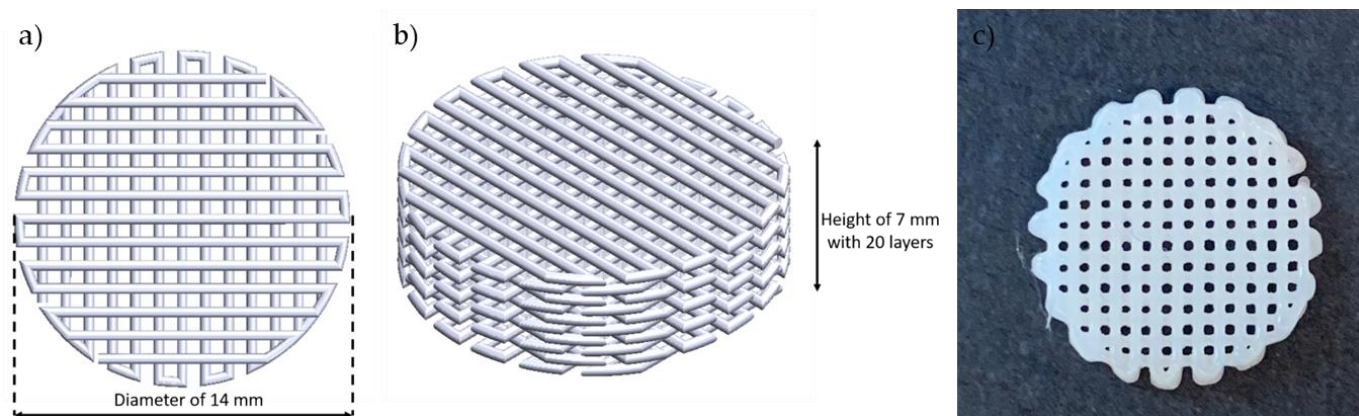


Figure 2. Scaffold design: (a) top view of designed scaffold, (b) isometric view of designed scaffold, and (c) top view of printed scaffold.

The degradation test of the scaffold was performed in an environment of PBS solution at 37 °C. Scaffolds fully soaked into a container containing PBS solution and the containers were stored in the vacuum oven for 9 weeks with interval 3 weeks. Every 3 weeks during the whole period of the test, the mass of the scaffolds was measured using a digital milligram scale (GEMINI-20, Cumming, GA, United States) in 1 mg increments. The degradation rate was evaluated by mass loss percent. All scaffold was cleaned and dried before measuring.

3. Results

3.1. Melting Temperature

In the DSC test result, the composites showed separated two peaks during the endothermic process while pure PCL and DMSO₂ showed only one peak (Figure 3). The melting temperatures of PCL in the composites ranged 55.99–56.73 °C, and it of DMSO₂ ranged 106.36–107.48 °C (Table 2). The temperature for specimen preparation was set as higher about 10%, 120 °C, because the specimen preparation process is not a closed system to be different from the DSC test condition.

3.2. Hydrophilicity of Composites

The hydrophilicity of PCL and DMSO₂ composites was better than it of pure PCL. The water contact angle (WCA) of PCL and DMSO₂ composites showed a decreasing angle value of 4.4, 10.2, and 15.5% compared to it of pure PCL according to the DMSO₂ concentration interval of 10 wt%, respectively (Figure 4). The WCA of PCL was 83.94°, and it of DMSO₂ was 43.35°, and PCL and DMSO₂ composites showed the WCA of 80.28°, 75.37°, and 70.96°, individually. This tendency was similarly observed in the PBS solution. The contact angle of PCL and DMSO₂ composites presented 78.63°, 74.05°, and 66.04° with 10, 20, and 30 wt% of DMSO₂ ratio, individually. All materials showed low contact angle in PBS solution (Figure 5).

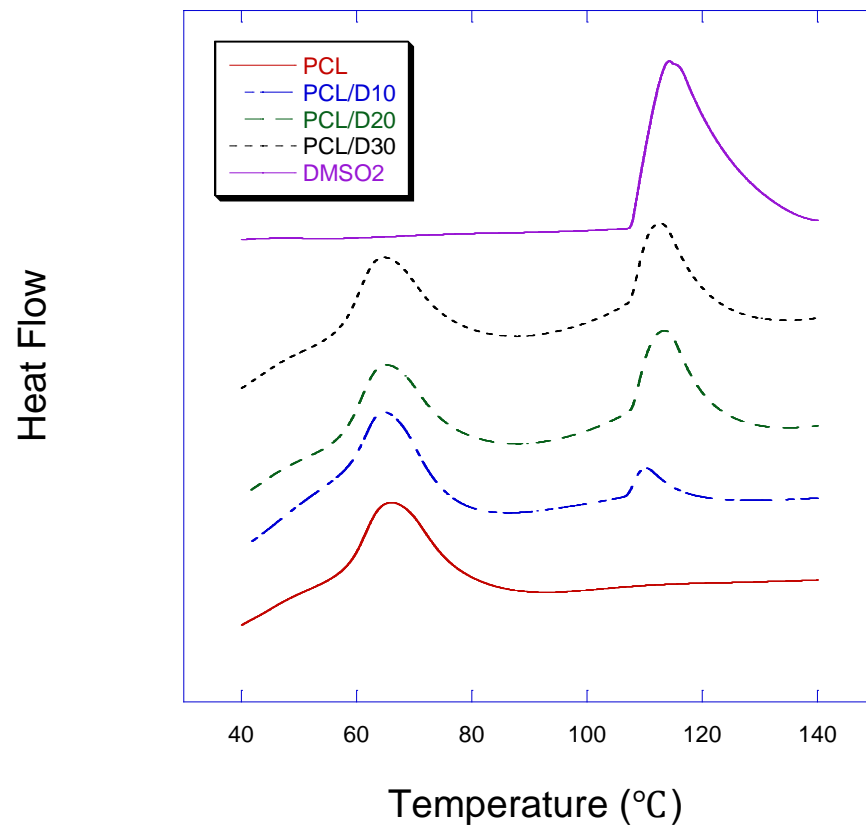


Figure 3. Dynamic DSC curves of PCL and DMSO₂ composites.

Table 2. Melting temperature measured by DSC curves.

Material	Melting Temperature (°C)				
	Mean	Peak 1	SD	Peak 2	SD
PCL	56.59		0.16		
PCL/D10	55.39		0.52	106.82	0.30
PCL/D20	56.40		0.20	106.67	0.31
PCL/D30	56.27		0.07	106.73	0.31
DMSO ₂				106.85	0.46

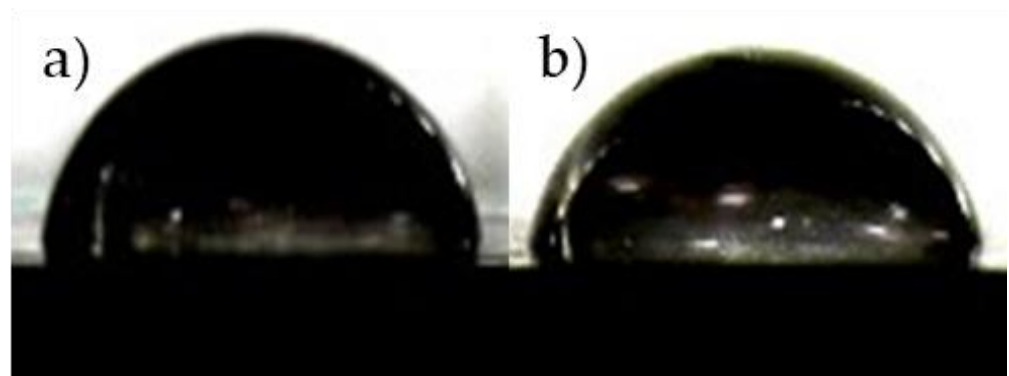


Figure 4. Water contact angles of PCL and DMSO₂ composites: (a) pure PCL and (b) PCL/D30.

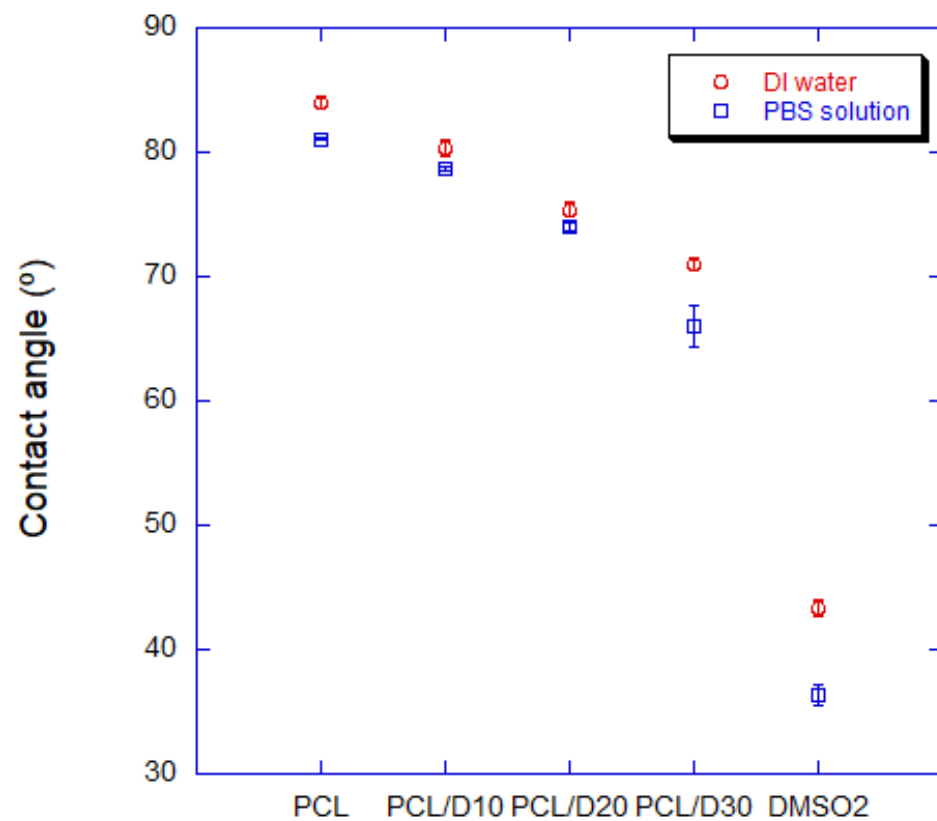


Figure 5. Contact angle of PCL and PCL/DMSO₂ composites with DI water and PBS solution.

3.3. Mechanical Properties

The elastic modulus of PCL and DMSO₂ composites showed a linear relationship with the DMSO₂ ratio with values of 440, 469, and 532 MPa at 10, 20, and 30 wt% of DMSO₂ concentration in composites (Table 3), individually. These results indicated improvement rates of 3.8, 10.6, and 25.5% at each composite compared to pure PCL. The stress-strain curves in the elastic region were shown in Figure 6. It is clear that the addition of DMSO₂ into PCL resulting in a positive change in the elastic modulus. The composites of PCL and DMSO₂ can be considered as particle reinforced polymer matrix composites. Many researchers studied on the mechanical properties of particle reinforced polymer matrix composites [54–57]. Mechanical properties can be accordingly enhanced by adding micro- or nano-sized particles because most rigid particles have a higher stiffness than natural or synthetic polymer matrices [58,59].

Table 3. Elastic modulus and 0.2% offset yield strength of PCL and PCL/DMSO₂ composites.

Material	Modulus in Elasticity (MPa)				0.2% Offset Yield Strength (MPa)			
	PCL	PCL/D10	PCL/D20	PCL/D30	PCL	PCL/D10	PCL/D20	PCL/D30
Mean	424	440	469	532	13.70	11.08	9.67	8.73
SD	2.94	1.41	5.35	5.35	0.44	0.25	0.41	0.22

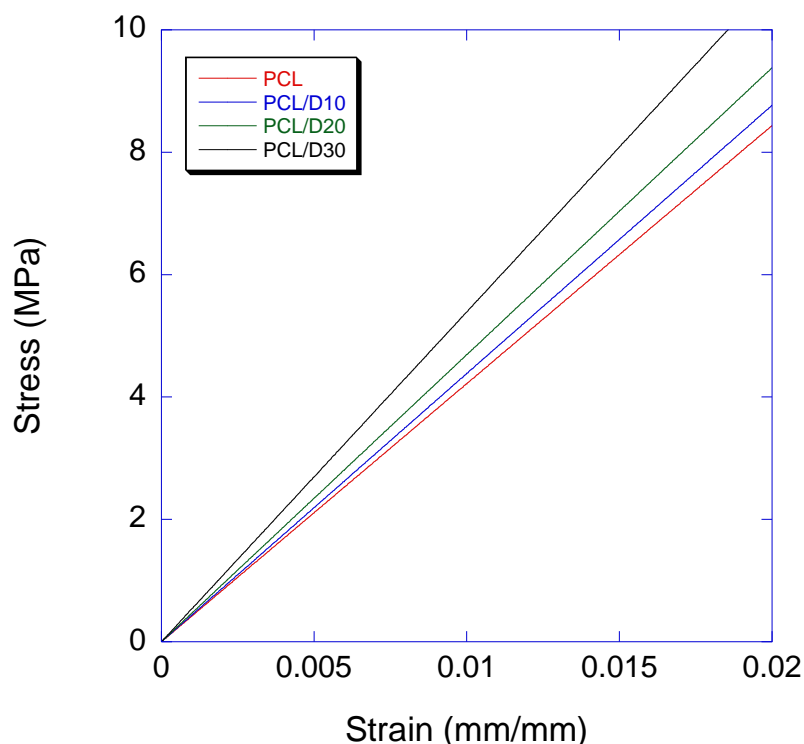


Figure 6. Stress-Strain curve of PCL and PCL/DMSO₂ composites in the elastic region.

In contrast to the positive relationship in elastic modulus between PCL and DMSO₂, 0.2% offset yield strength of PCL and DMSO₂ composites were decreased with increasing DMSO₂ ratio. Strength including yield strength heavily depends on the stress transfer between polymer matrix and added particle, and well-bonded polymer matrix and particle can transfer enforced stress through the interface from polymer to the particle [60]. This process can clearly improve strength. In poor interface adhesion between polymer and particle, declined strength, however, could appear in composites, and this phenomenon occurs in micro-particle more frequently than nano-particle [61]. To observe interface adhesion, scanning electron microscope (SEM) analysis was conducted.

The PCL and DMSO₂ composites showed a clear surface without any defects (Figure 7). DMSO₂ particles were pulled out from the PCL matrix due to low interface adhesion during the mechanical test, and stress is concentrated on the void. Stress concentrated void extended, and the fracture happened, finally. The evidence of pulling out of DMSO₂ from PCL can be seen on the fracture surface.

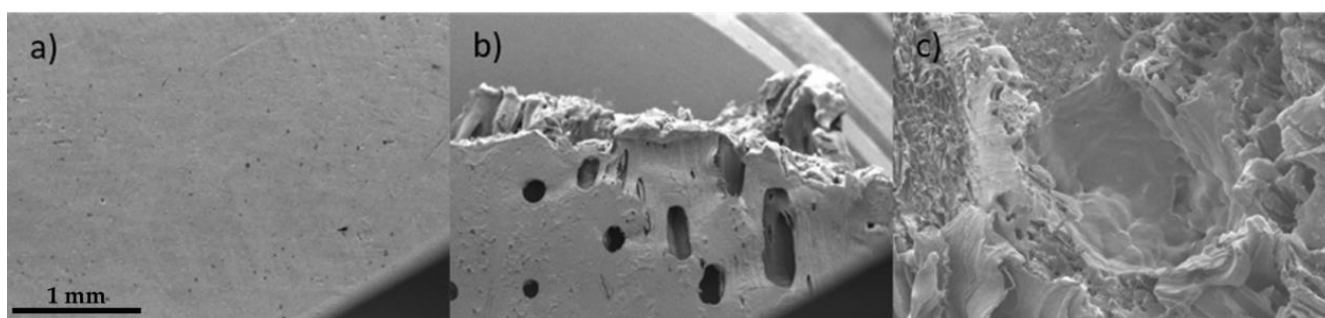


Figure 7. SEM images of PCL and DMSO₂ composite with magnification $\times 50$ (a) surface before mechanical test, (b) side view after mechanical test, and (c) top view after mechanical test.

3.4. Degradation Property In Vitro

Three samples were tested for each composition, and mean values and standard deviations were proposed. After 9 weeks, the mass of pure PCL decreased a total of 1.62%, and it almost linearly decreased by 0.61% every 3 weeks on average. On the other hand, the mass loss of PCL and DMSO₂ composites noticeably increased compared to pure PCL. The final mass losses of composites were totals of 7.29, 17.67, and 29.40% with 10, 20, and 30 wt% of DMSO₂ concentration, respectively, and the mass loss was apparently faster in the first 3 weeks; after that, the mass loss rate gradually decreased until the end of the 9 weeks. Degradation rate by measuring mass loss was shown in Figure 8 and Table 4.

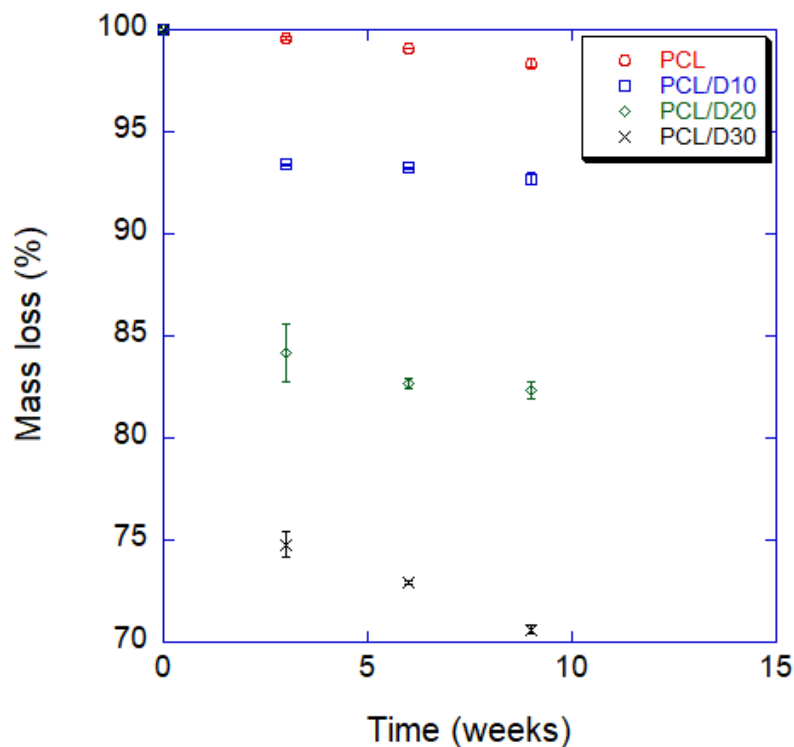


Figure 8. Mass loss for 9 weeks with interval 3 weeks of PCL and PCL/DMSO₂ composites.

Table 4. Mass loss value and standard deviation of PCL and composites for 9 weeks.

Weeks	PCL		PCL/D10		PCL/D20		PCL/D30	
	Mean	SD	Mean	SD	Mean	SD	Mean	SD
0	100		100		100		100	
3	99.60	0.07	93.40	0.02	84.19	1.43	74.79	0.60
6	99.09	0.01	93.23	0.06	82.67	0.23	72.91	0.10
9	98.38	0.17	92.71	0.26	82.33	0.45	70.60	0.21

4. Discussion

The wettability of a polymer can be affected by its physical properties, particularly surface free energy. Therefore, it is possible to obtain PCL with varying molecular weights, resulting in different surface free energy and water contact angle [62,63]. In this study, PCL with 50,000 molecular weight was tested, and the literature data [64] used PCL with 80,000 molecular weight. This is the reason why the water contact angles of the literature data and the current study are different. High contact angle of pure PCL is caused by low surface energy which interrupts initial cell adhesion, leading to limit cell to cell or cell to matrix interactions [30,65]. DMSO₂ can play a role reducing the liquid contact angle due to high surface energy and improving the process of cell attachment by adding to PCL

matrix. Adding the DMSO₂ in the PCL on hydrophilicity is better than other PCL-based composites. Moreover, the result of PCL/DMSO₂ 30 wt% composite indicates the WCA of the composite can reach metallic biomaterial level such as titanium, although polymers generally show higher contact angle compared to that of ceramics and metals due to the surface energy difference (Table 5).

Table 5. Water contact angle of various biomaterials.

Group	Materials	Water Contact Angle (°)	Refs.	
Metal	Magnesium	40.8	[66]	
	Tantalum	61	[67]	
	Titanium	73	[68]	
Ceramic	Alumina	64.74	[69]	
	Zirconia	65	[70]	
Natural Polymer	Collagen	62.17	[71]	
	Gelatin	78.6	[72]	
	Chitosan	80	[73]	
Polymer	PLA ¹	87.2	[74]	
	Synthetic Polymer	PCL	83.9	Current study
		PGA ²	118	
		PLGA ³	109.8	
		124.9		

¹ polylactic acid; ² polyglycolide; ³ Polylactic-co-glycolic acid.

The contact angle of bio composite material can be calculated by young's equation [77] and rule of mixture. Young's equation relating surface energy of a solid, surface tension of a liquid and the interfacial tension between the liquid and solid is related to the contact angle as follows,

$$\sigma_s = \sigma_{sl} + \sigma_l \cos \theta \quad (4)$$

where, σ_s is surface energy of a solid, σ_{sl} is the interfacial tension between the liquid and solid, σ_l is surface tension of a liquid, and θ is the contact angle. Therefore, both the surface energy of a solid and the contact angle are closely related. Fowkes [78] proposed a simple equation to deal with the σ_{sl} as function of σ_s and σ_l in the following way,

$$\sigma_{sl} = \sigma_s + \sigma_l - 2\sqrt{\sigma_s \sigma_l} \quad (5)$$

Combining Equations (4) and (5) to eliminate the term of σ_{sl} and applying a general rule of mixtures, the contact angle can be predicted like Equation (6).

$$\theta = \cos^{-1} \left(-1 + 2\sqrt{\frac{\sigma_{PCL}(1-f) + \sigma_{DMSO_2}f}{\sigma_l}} \right) \quad (6)$$

where σ_{PCL} and σ_{DMSO_2} are solid surface energy of PCL and DMSO₂, respectively, and f is the fraction of DMSO₂ in PCL and DMSO₂ composites. Experiment contact angle value and predicted curve with DI water were shown in Figure 9. Coefficient of determination (R^2) of predicted curve was 0.9116.

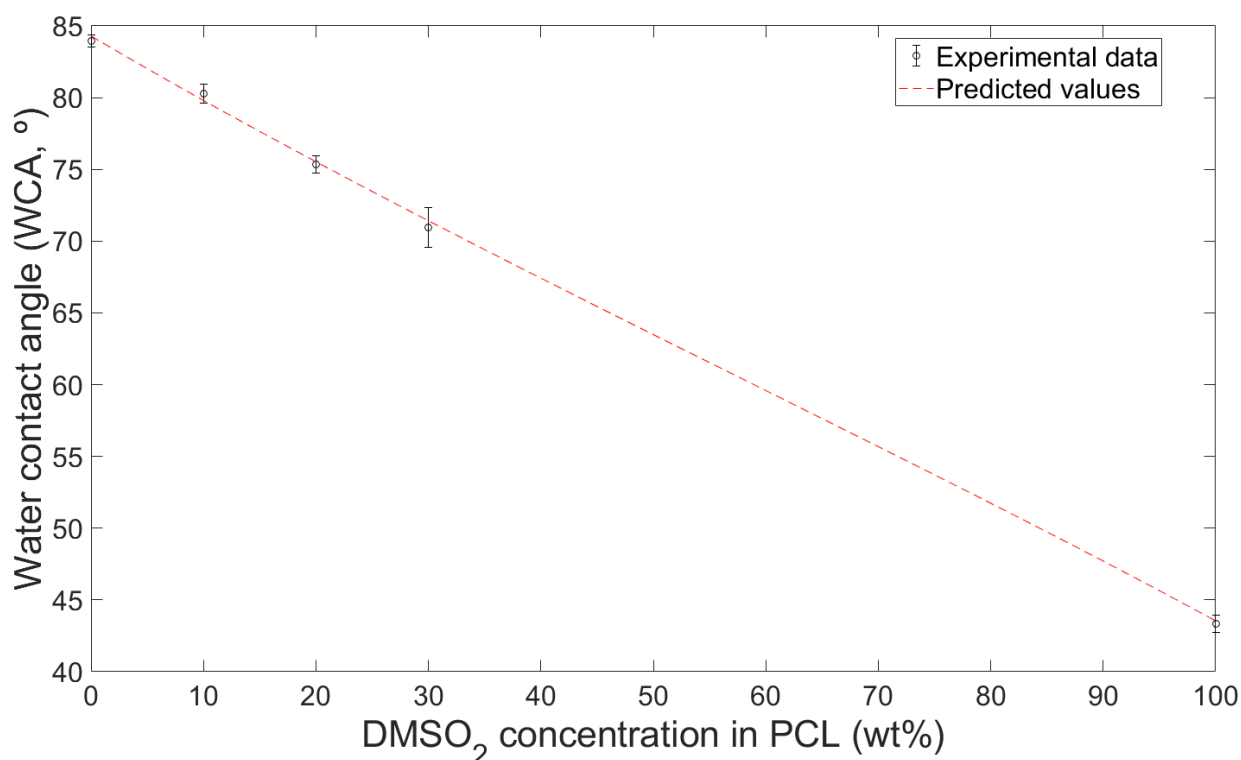


Figure 9. Contact angle with DI water of experiment value and predicted curve.

Hydrophilicity of biomaterial can be enhanced by surface treatment including etching, blasting, passivation, and plasma as well as blending other materials [79,80]. Strnad et al. [79] reported the surface treatment effects of acid etching, sandblasting, passivation, and their combinations on the titanium-based biomaterials. Long acid etching times affected a positive effect on hydrophilicity, but sandblasting did not influence significantly. Xu et al. [80] noted plasma surface treatment with time. After 150 min, the contact angle showed almost half the value compared with the initial contact angle. The hydrophilicity of PCL and DMSO₂ composites might be more improved by surface treatment such as plasma treatment without changing DMSO₂ concentration.

The elastic modulus of the single biomaterial, such as biopolymer, can be improved by fabricating composite material (Table 6), and the modulus is highly affected by test specimen design and additive materials [13,18]. PCL has a wide range of molecular weight, and thus the range of mechanical properties is also varied [62,81,82]. Perstorp (Malmö, Sweden) announced bulk PCL with a molecular weight of 50,000 had an elastic modulus of 470 MPa and 0.2% offset yield strength of 17.5 MPa [83]. However, PCL shows relatively low modulus compared to other synthetic biopolymers such as PLA and PGA [84]. Doyle et al. [85] studied the mechanical properties of PCL and nano-hydroxyapatite (nHA) blends with cylindrical disk specimens (7 mm diameter, 2 mm height) in the compressive test. The nHA showed negative effect in the low nHA concentration (10%), but in the high nHA concentration (30%) indicated higher modulus than PCL. Germiniani et al. [86] published about PCL and cellulose nanocrystals (CNC) composites. The mechanical test was performed according to ASTM D882-10. The modulus of composites was increased with CNC concentration, but in the CNC of 5%, the modulus was decreased. However, the modulus of PCL and DMSO₂ composites was increased regardless of DMSO₂ concentration unlike other additives.

Table 6. Elastic modulus of PCL based composites.

Polymer Matrix	Additive	Additive Ratio (%)	Specimen	Test Method	Modulus (Mpa)	Refs.
PCL	-	-	Solid	Tensile test	440	[83]
	-	-	Solid	Three-point bending	414	[83]
	-	-	Solid	Compressive test	455	[83]
	-	-	Scaffold	Compressive test	10	[83]
	DMSO ₂	10	Molded bar	Three-point bending	440	Current study
	DMSO ₂	20	Molded bar	Three-point bending	469	Current study
	DMSO ₂	30	Molded bar	Three-point bending	532	Current study
	nHA ¹	0	Cylindrical disk	Compressive test	71.72	[85]
	nHA	10	Cylindrical disk	Compressive test	67.65	[85]
	nHA	30	Cylindrical disk	Compressive test	68.55	[85]
	CNC ²	0	nano fiber	-	23.4	[49]
	CNC	0	nano fiber	-	33.1	[49]
	CNC	1	nano fiber	-	43.8	[49]
	CNC	1.5	nano fiber	-	39	[49]
	CNC	2.5	nano fiber	-	39.6	[49]
	CNC	4	nano fiber	-	27.8	[49]
	CNC	0	-	-	246.45	[86]
	CNC	5	-	-	205.95	[86]
	CNC	10	-	-	313.55	[86]
	CNC	15	-	-	460.5	[86]
	CNC	20	-	-	500.99	[86]
	CNC	25	-	-	629.42	[86]
	-	-	Scaffold	-	3.58	[87]
	MTA ³	-	Scaffold	-	4.07	[87]
	PCL grafted CNC	0	nano fiber	-	4.09	[88]
	PCL grafted CNC	1	nano fiber	-	4.49	[88]
	PCL grafted CNC	3	nano fiber	-	6.01	[88]
	PCL grafted CNC	5	nano fiber	-	6.94	[88]

¹ nano hydroxyapatite; ² cellulose nanocrystals; ³ mineral trioxide aggregate.

DMSO₂ is an organic sulfur, and the efficient breakdown of sulfide ions allows for further degradation of organic pollutants at an acidic pH, resulting in a highly effective treatment process [89]. This study showed that the degradation time of PCL and DMSO₂ composite can tailor according to the DMSO₂ ratio. A tailorable degradation time of the biomaterial can expand the use of the biomaterial because the human tissues have different regeneration times depending on the tissue and the extent of the wound [90,91]. In this study, the degradation time of the composites is reduced up to 18 times with DMSO₂ of 30% after 9 weeks. The degradation time can be tailored more precisely by controlling the content of DMSO₂ in the composites.

5. Conclusions

The purpose of this study was to develop a new bio-scaffold material using PCL and DMSO₂ composites, and to investigate the hydrophilicity, mechanical, and degradation properties of the resulting materials. The experimental results showed that the PCL and DMSO₂ composites had improved hydrophilicity and mechanical properties compared to pure PCL, and their degradation properties were tunable by regulating the concentration of DMSO₂ in the PCL matrix.

1. The water contact angle decreased by 4.4%, 10.2%, and 15.5% with 10%, 20%, and 30 wt%, respectively, while the contact angle with PBS solution decreases 3.0%, 8.7%, and 18.5% with those. The water contact angle of the composites can be predicted using the surface tension of each material.
2. Adding DMSO₂ to the PCL matrix increased the elastic modulus with increasing DMSO₂ concentration rate. However, the 0.2% offset yield strength decreased with increasing DMSO₂ ratio due to poor interfacial adhesion between PCL and DMSO₂, which occurred more frequently with micro-sized particles than with nano-sized particles. The addition of extra additives, such as a binder, can be used to improve the yield strengths of the composites. The degradation rate should be regulated for specific conditions.
3. The degradation time of the composite with 30 wt% of DMSO₂ was 18 times faster than that of pure PCL in a 9 week test. PCL and DMSO₂ composites can tailor the degraded rate with DMSO₂ ratio, and a wide range of degradation time can increase the selection for applications.

According to the above results, DMSO₂ can play a role of increasing hydrophilicity, elastic modulus, and decreasing degradation time in the composites. Newly developed PCL/DMSO₂ composites can be used as a bio-scaffold material in tissue engineering field.

Author Contributions: Conceptualization, J.-W.J., K.-E.M., C.K., C.W. and S.Y.; methodology, J.-W.J., K.-E.M., C.K., C.W. and S.Y.; investigation, J.-W.J., K.-E.M., C.K., C.W. and S.Y.; writing—original draft preparation, J.-W.J., writing—review and editing, C.K. and S.Y.; project administration, S.Y. All authors have read and agreed to the published version of the manuscript.

Funding: This study has been conducted with the support of the Korea Institute of Industrial Technology as “Development of controllable mechanical and biological properties scaffold based on additive manufacturing (KITECH JE-22-0012)”.

Institutional Review Board Statement: Not applicable.

Informed Consent Statement: Not applicable.

Data Availability Statement: The data presented in this study are available on request from the corresponding author.

Conflicts of Interest: The authors declare no conflict of interest.

References

1. Salgado, A.J.; Coutinho, O.P.; Reis, R.L. Bone tissue engineering: State of the art and future trends. *Macromol. Biosci.* **2004**, *4*, 743–765. [[CrossRef](#)] [[PubMed](#)]
2. Amini, A.R.; Laurencin, C.T.; Nukavarapu, S.P. Bone tissue engineering: Recent advances and challenges. *Crit. Rev. Biomed. Eng.* **2012**, *40*, 363–408. [[CrossRef](#)] [[PubMed](#)]
3. Black, C.R.; Goriainov, V.; Gibbs, D.; Kanczler, J.; Tare, R.S.; Oreffo, R.O. Bone tissue engineering. *Curr. Mol. Biol. Rep.* **2015**, *1*, 132–140. [[CrossRef](#)] [[PubMed](#)]
4. Turner, C.H.; Burr, D.B. Basic biomechanical measurements of bone: A tutorial. *Bone* **1993**, *14*, 595–608. [[CrossRef](#)] [[PubMed](#)]
5. Li, L.; Lu, H.; Zhao, Y.; Luo, J.; Yang, L.; Liu, W.; He, Q. Functionalized cell-free scaffolds for bone defect repair inspired by self-healing of bone fractures: A review and new perspectives. *Mater. Sci. Eng. C* **2019**, *98*, 1241–1251. [[CrossRef](#)] [[PubMed](#)]
6. Boyce, T.; Edwards, J.; Scarborough, N. Allograft bone: The influence of processing on safety and performance. *Orthop. Clin.* **1999**, *30*, 571–581.
7. Baldwin, P.; Li, D.J.; Auston, D.A.; Mir, H.S.; Yoon, R.S.; Koval, K.J. Autograft, allograft, and bone graft substitutes: Clinical evidence and indications for use in the setting of orthopaedic trauma surgery. *J. Orthop. Trauma* **2019**, *33*, 203–213. [[CrossRef](#)]
8. Migliorini, F.; La Padula, G.; Torsiello, E.; Spiezia, F.; Oliva, F.; Maffulli, N. Strategies for large bone defect reconstruction after trauma, infections or tumour excision: A comprehensive review of the literature. *Eur. J. Med. Res.* **2021**, *26*, 118. [[CrossRef](#)]
9. Khush, K.K.; Menza, R.; Nguyen, J.; Zaroff, J.G.; Goldstein, B.A. Donor predictors of allograft use and recipient outcomes after heart transplantation. *Circ. Heart Fail.* **2013**, *6*, 300–309. [[CrossRef](#)]
10. Marew, T.; Birhanu, G. Three dimensional printed nanostructure biomaterials for bone tissue engineering. *Regen. Ther.* **2021**, *18*, 102–111. [[CrossRef](#)]

11. Ren, J.; Xu, Y.; Zhiyi, G.; Ren, T.; Ren, J.; Wang, K.; Luo, Y.; Zhu, M.; Tan, Q. Reconstruction of the trachea and carina: Surgical reconstruction, autologous tissue transplantation, allograft transplantation, and bioengineering. *Thorac. Cancer* **2022**, *13*, 284–295. [[CrossRef](#)] [[PubMed](#)]
12. Organ Donation Statistics. 2021. Available online: <https://www.organdonor.gov/learn/organ-donation-statistics> (accessed on 9 January 2022).
13. Hollister, S.J. Porous scaffold design for tissue engineering. *Nat. Mater.* **2005**, *4*, 518–524. [[CrossRef](#)]
14. Frantz, C.; Stewart, K.M.; Weaver, V.M. The extracellular matrix at a glance. *J. Cell Sci.* **2010**, *123*, 4195–4200. [[CrossRef](#)] [[PubMed](#)]
15. Nair, L.S.; Laurencin, C.T. Biodegradable polymers as biomaterials. *Prog. Polym. Sci.* **2007**, *32*, 762–798. [[CrossRef](#)]
16. Mitragotri, S.; Lahann, J. Physical approaches to biomaterial design. *Nat. Mater.* **2009**, *8*, 15–23. [[CrossRef](#)] [[PubMed](#)]
17. Marin, E.; Boschetto, F.; Pezzotti, G. Biomaterials and biocompatibility: An historical overview. *J. Biomed. Mater. Res. Part A* **2020**, *108*, 1617–1633. [[CrossRef](#)]
18. Hutmacher, D.W. Scaffold design and fabrication technologies for engineering tissues—State of the art and future perspectives. *J. Biomater. Sci. Polym. Ed.* **2001**, *12*, 107–124. [[CrossRef](#)] [[PubMed](#)]
19. Hutmacher, D.W.; Woodfield, T.B.; Dalton, P.D. Scaffold design and fabrication. In *Tissue Engineering*; Elsevier: Amsterdam, The Netherlands, 2014; pp. 311–346.
20. Collins, M.N.; Ren, G.; Young, K.; Pina, S.; Reis, R.L.; Oliveira, J.M. Scaffold fabrication technologies and structure/function properties in bone tissue engineering. *Adv. Funct. Mater.* **2021**, *31*, 2101069. [[CrossRef](#)]
21. Tathe, A.; Ghodke, M.; Nikalje, A.P. A brief review: Biomaterials and their application. *Int. J. Pharm. Pharm. Sci.* **2010**, *2*, 19–23.
22. Black, J.; Hastings, G. *Handbook of Biomaterial Properties*; Springer Science & Business Media: New York, NY, USA, 2013.
23. Okamoto, M.; John, B. Synthetic biopolymer nanocomposites for tissue engineering scaffolds. *Prog. Polym. Sci.* **2013**, *38*, 1487–1503. [[CrossRef](#)]
24. Sampath, U.G.T.; Ching, Y.C.; Chuah, C.H.; Sabariah, J.J.; Lin, P.-C. Fabrication of porous materials from natural/synthetic biopolymers and their composites. *Materials* **2016**, *9*, 991. [[CrossRef](#)] [[PubMed](#)]
25. Mtibe, A.; Motloug, M.P.; Bandyopadhyay, J.; Ray, S.S. Synthetic biopolymers and their composites: Advantages and limitations—An overview. *Macromol. Rapid Commun.* **2021**, *42*, 2100130. [[CrossRef](#)] [[PubMed](#)]
26. Farah, S.; Anderson, D.G.; Langer, R. Physical and mechanical properties of PLA, and their functions in widespread applications—A comprehensive review. *Adv. Drug Deliv. Rev.* **2016**, *107*, 367–392. [[CrossRef](#)] [[PubMed](#)]
27. Malikmammadov, E.; Tanir, T.E.; Kiziltay, A.; Hasirci, V.; Hasirci, N. PCL and PCL-based materials in biomedical applications. *J. Biomater. Sci. Polym. Ed.* **2018**, *29*, 863–893. [[CrossRef](#)]
28. Patrício, T.; Domingos, M.; Gloria, A.; D’Amora, U.; Coelho, J.; Bártolo, P. Fabrication and characterisation of PCL and PCL/PLA scaffolds for tissue engineering. *Rapid Prototyp. J.* **2014**, *20*, 145–156. [[CrossRef](#)]
29. Carmona, V.B.; Corrêa, A.C.; Marconcini, J.M.; Mattoso, L.H.C. Properties of a biodegradable ternary blend of thermoplastic starch (TPS), poly (ϵ -caprolactone)(PCL) and poly (lactic acid)(PLA). *J. Polym. Environ.* **2015**, *23*, 83–89. [[CrossRef](#)]
30. Agrawal, G.; Negi, Y.S.; Pradhan, S.; Dash, M.; Samal, S. Wettability and contact angle of polymeric biomaterials. In *Characterization of Polymeric Biomaterials*; Elsevier: Amsterdam, The Netherlands, 2017; pp. 57–81.
31. Udofia, E.N.; Zhou, W. Microextrusion based 3D printing—A review. In proceeding of the 2018 International Solid Freeform Fabrication Symposium—An Additive Manufacturing Conference, Austin, TX, USA, 13–15 August 2018.
32. Wong, T.; Bloomer, R.J.; Benjamin, R.L.; Buddington, R.K. Small intestinal absorption of methylsulfonylmethane (MSM) and accumulation of the sulfur moiety in selected tissues of mice. *Nutrients* **2017**, *10*, 19. [[CrossRef](#)]
33. Hewlings, S.; Kalman, D. Sulfur in human health. *EC Nutr.* **2019**, *14*, 785–791.
34. Maraño, G.; Muñoz-Escassi, B.; Manley, W.; García, C.; Cayado, P.; De la Muela, M.S.; Olábarri, B.; León, R.; Vara, E. The effect of methyl sulphonyl methane supplementation on biomarkers of oxidative stress in sport horses following jumping exercise. *Acta Vet. Scand.* **2008**, *50*, 45. [[CrossRef](#)]
35. Kim, L.S.; Axelrod, L.; Howard, P.; Buratovich, N.; Waters, R. Efficacy of methylsulfonylmethane (MSM) in osteoarthritis pain of the knee: A pilot clinical trial. *Osteoarthr. Cartil.* **2006**, *14*, 286–294. [[CrossRef](#)]
36. Loeser, R.F.; Goldring, S.R.; Scanzello, C.R.; Goldring, M.B. Osteoarthritis: A disease of the joint as an organ. *Arthritis Rheum.* **2012**, *64*, 1697. [[CrossRef](#)] [[PubMed](#)]
37. Carballo, C.B.; Nakagawa, Y.; Sekiya, I.; Rodeo, S.A. Basic science of articular cartilage. *Clin. Sport. Med.* **2017**, *36*, 413–425. [[CrossRef](#)] [[PubMed](#)]
38. Ezaki, J.; Hashimoto, M.; Hosokawa, Y.; Ishimi, Y. Assessment of safety and efficacy of methylsulfonylmethane on bone and knee joints in osteoarthritis animal model. *J. Bone Miner. Metab.* **2013**, *31*, 16–25. [[CrossRef](#)] [[PubMed](#)]
39. Abdel-Rafei, M.K.; Thabet, N.M. Modulatory effect of methylsulfonylmethane against BPA/ γ -radiation induced neurodegenerative alterations in rats: Influence of TREM-2/DAP-12/Syk pathway. *Life Sci.* **2020**, *260*, 118410. [[CrossRef](#)]
40. Máca, J.; Vondrák, J.; Sedlářková, M. Use of Dimethyl Sulfone as Additive in Aprotic Electrolytes. *ECS Trans.* **2014**, *48*, 135. [[CrossRef](#)]
41. Markaryan, S.A.; Aznauryan, M.; Kazoyan, E. Physicochemical properties of aqueous solutions of dimethyl- and diethylsulfones. *Russ. J. Phys. Chem. A* **2011**, *85*, 2138–2141. [[CrossRef](#)]
42. Markuniene, I.; Rabiei, M.; Nasiri, S.; Urbaite, S.; Palevicius, A.; Janusas, G. Biocompatible Piezoelectric PVDF/HA/AgNO₃ Thin Film Prepared by the Solvent Casting Method. *Sensors* **2022**, *23*, 289. [[CrossRef](#)]

43. Gautam, S.; Sharma, C.; Purohit, S.D.; Singh, H.; Dinda, A.K.; Potdar, P.D.; Chou, C.-F.; Mishra, N.C. Gelatin-polycaprolactone-nanohydroxyapatite electrospun nanocomposite scaffold for bone tissue engineering. *Mater. Sci. Eng. C* **2021**, *119*, 111588. [[CrossRef](#)]
44. Murugan, S.; Parcha, S.R. Fabrication techniques involved in developing the composite scaffolds PCL/HA nanoparticles for bone tissue engineering applications. *J. Mater. Sci. Mater. Med.* **2021**, *32*, 93. [[CrossRef](#)]
45. Petretta, M.; Gambardella, A.; Desando, G.; Cavallo, C.; Bartolotti, I.; Shelyakova, T.; Goranov, V.; Brucale, M.; Dediu, V.A.; Fini, M. Multifunctional 3D-printed magnetic polycaprolactone/hydroxyapatite scaffolds for bone tissue engineering. *Polymers* **2021**, *13*, 3825. [[CrossRef](#)]
46. Wang, F.; Tankus, E.B.; Santarella, F.; Rohr, N.; Sharma, N.; Martin, S.; Michalscheck, M.; Maintz, M.; Cao, S.; Thieringer, F.M. Fabrication and characterization of PCL/HA filament as a 3D printing material using thermal extrusion technology for bone tissue engineering. *Polymers* **2022**, *14*, 669. [[CrossRef](#)] [[PubMed](#)]
47. Bakhsheshi-Rad, H.R.; Hamzah, E.; Ying, W.S.; Razzaghi, M.; Sharif, S.; Ismail, A.F.; Berto, F. Improved bacteriostatic and anticorrosion effects of polycaprolactone/chitosan coated magnesium via incorporation of zinc oxide. *Materials* **2021**, *14*, 1930. [[CrossRef](#)] [[PubMed](#)]
48. Liu, D.; Nie, W.; Li, D.; Wang, W.; Zheng, L.; Zhang, J.; Zhang, J.; Peng, C.; Mo, X.; He, C. 3D printed PCL/SrHA scaffold for enhanced bone regeneration. *Chem. Eng. J.* **2019**, *362*, 269–279. [[CrossRef](#)]
49. Hivechi, A.; Bahrami, S.H.; Siegel, R.A. Drug release and biodegradability of electrospun cellulose nanocrystal reinforced polycaprolactone. *Mater. Sci. Eng. C Mater. Biol. Appl.* **2019**, *94*, 929–937. [[CrossRef](#)]
50. Min, K.-E.; Kim, H.-Y.; Bang, J.-H.; Kim, J.-H.; Kim, J.-K. Effects of Hardeners and Catalysts on the Reliability of Copper to Copper Adhesive Joint. *Korean J. Mater. Res.* **2011**, *21*, 283–287. [[CrossRef](#)]
51. Min, K.-E.; Jang, J.-W.; Kim, J.-K.; Wern, C.; Yi, S. Thermophysical Properties of Inorganic Phase-Change Materials Based on MnCl₂·4H₂O. *Appl. Sci.* **2022**, *12*, 6338. [[CrossRef](#)]
52. ASTM D790; Standard Test Methods for Flexural Properties of Unreinforced and Reinforced Plastics and Electrical Insulating Materials. Annual Book of ASTM Standards: West Conshohocken, PA, USA, 1997. Available online: <https://www.astm.org/d0790-17.html> (accessed on 15 December 2022).
53. ASTM D7334-08; ASTM Standards. Standard Practice for Surface Wettability of Coatings, Substrates and Pigments by Advancing Contact Angle Measurement. Annual Book of ASTM Standards: West Conshohocken, PA, USA, 2013. Available online: <https://www.astm.org/d7334-08r22.html> (accessed on 15 December 2022).
54. Haibach, K.; Menner, A.; Powell, R.; Bismarck, A. Tailoring mechanical properties of highly porous polymer foams: Silica particle reinforced polymer foams via emulsion templating. *Polymer* **2006**, *47*, 4513–4519. [[CrossRef](#)]
55. Robertson, C.G.; Lin, C.; Rackaitis, M.; Roland, C. Influence of particle size and polymer–filler coupling on viscoelastic glass transition of particle-reinforced polymers. *Macromolecules* **2008**, *41*, 2727–2731. [[CrossRef](#)]
56. Chandramohan, D.; Rajesh, S. Study of machining parameters on natural fiber particle reinforced polymer composite material. *Acad. J. Manuf. Eng.* **2014**, *12*, 72–77.
57. Chandramohan, D.; Kumar, A.J.P. Experimental data on the properties of natural fiber particle reinforced polymer composite material. *Data Brief* **2017**, *13*, 460–468. [[CrossRef](#)]
58. Jose, A.S.; Athijayamani, A.; Jani, S. A review on the mechanical properties of bio waste particulate reinforced polymer composites. *Mater. Today Proc.* **2021**, *37*, 1757–1760. [[CrossRef](#)]
59. Kuan, H.T.N.; Tan, M.Y.; Shen, Y.; Yahya, M.Y. Mechanical properties of particulate organic natural filler-reinforced polymer composite: A review. *Compos. Adv. Mater.* **2021**, *30*, 1–17. [[CrossRef](#)]
60. Fu, S.-Y.; Feng, X.-Q.; Lauke, B.; Mai, Y.-W. Effects of particle size, particle/matrix interface adhesion and particle loading on mechanical properties of particulate–polymer composites. *Compos. Part B Eng.* **2008**, *39*, 933–961. [[CrossRef](#)]
61. Chawla, N.; Sidhu, R.; Ganesh, V. Three-dimensional visualization and microstructure-based modeling of deformation in particle-reinforced composites. *Acta Mater.* **2006**, *54*, 1541–1548. [[CrossRef](#)]
62. Hendrikson, W.; Rouwkema, J.; Van Blitterswijk, C.; Moroni, L. Influence of PCL molecular weight on mesenchymal stromal cell differentiation. *RSC Adv.* **2015**, *5*, 54510–54516. [[CrossRef](#)]
63. Kołbuk, D.; Ciechomska, M.; Jeznach, O.; Sajkiewicz, P. Effect of crystallinity and related surface properties on gene expression of primary fibroblasts. *RSC Adv.* **2022**, *12*, 4016–4028. [[CrossRef](#)]
64. Ayyoob, M.; Kim, Y.J. Effect of Chemical Composition Variant and Oxygen Plasma Treatments on the Wettability of PLGA Thin Films, Synthesized by Direct Copolycondensation. *Polymers* **2018**, *10*, 1132. [[CrossRef](#)]
65. Menzies, K.L.; Jones, L. The impact of contact angle on the biocompatibility of biomaterials. *Optom. Vis. Sci.* **2010**, *87*, 387–399. [[CrossRef](#)]
66. Cheon, K.H.; Park, C.; Kang, M.H.; Kang, I.G.; Lee, M.K.; Lee, H.; Kim, H.E.; Jung, H.D.; Jang, T.S. Construction of tantalum/poly(ether imide) coatings on magnesium implants with both corrosion protection and osseointegration properties. *Bioact. Mater.* **2021**, *6*, 1189–1200. [[CrossRef](#)]
67. Minagar, S.; Berndt, C.C.; Wen, C. Fabrication and Characterization of Nanoporous Niobia, and Nanotubular Tantalum, Titania and Zirconia via Anodization. *J. Funct. Biomater.* **2015**, *6*, 153–170. [[CrossRef](#)]
68. Ding, Z.; Wang, Y.; Zhou, Q.; Ding, Z.; Wu, Y.; Zhu, Y.; Shi, W.; He, Q. The Preparation and Properties of Multilayer Cu-MTa₂O₅ Composite Coatings on Ti6Al4V for Biomedical Applications. *Nanomaterials* **2019**, *9*, 1498. [[CrossRef](#)] [[PubMed](#)]

69. Yoon, S.Y.; Jeon, H.; Yi, C.; Park, S.; Ryu, S.; Kim, S.B. Mutual Interaction between Plasma Characteristics and Liquid Properties in AC-driven Pin-to-Liquid Discharge. *Sci. Rep.* **2018**, *8*, 12037. [[CrossRef](#)] [[PubMed](#)]
70. Wu, C.C.; Wei, C.K.; Ho, C.C.; Ding, S.J. Enhanced Hydrophilicity and Biocompatibility of Dental Zirconia Ceramics by Oxygen Plasma Treatment. *Materials* **2015**, *8*, 684–699. [[CrossRef](#)]
71. Chen, X.; Meng, J.; Xu, H.; Shinoda, M.; Kishimoto, M.; Sakurai, S.; Yamane, H. Fabrication and Properties of Electrospun Collagen Tubular Scaffold Crosslinked by Physical and Chemical Treatments. *Polymers* **2021**, *13*, 755. [[CrossRef](#)]
72. Li, Y.; Ceylan, M.; Shrestha, B.; Wang, H.; Lu, Q.R.; Asmatulu, R.; Yao, L. Nanofibers support oligodendrocyte precursor cell growth and function as a neuron-free model for myelination study. *Biomacromolecules* **2014**, *15*, 319–326. [[CrossRef](#)] [[PubMed](#)]
73. Gholami, N.; Jaleh, B.; Golbedaghi, R.; Larijani, M.M.; Wanichapichart, P.; Nasrollahzadeh, M.; Varma, R.S. Modification of Chitosan Membranes via Methane Ion Beam. *Molecules* **2020**, *25*, 2292. [[CrossRef](#)]
74. Ercan, U.K.; İbiş, F.; Dikyol, C.; Horzum, N.; Karaman, O.; Yıldırım, Ç.; Çukur, E.; Demirci, E.A. Prevention of bacterial colonization on nonthermal atmospheric plasma treated surgical sutures for control and prevention of surgical site infections. *PLoS ONE* **2018**, *13*, e0202703. [[CrossRef](#)]
75. Aghdam, R.M.; Najarian, S.; Shakhesi, S.; Khanlari, S.; Shaabani, K.; Sharifi, S. Investigating the effect of PGA on physical and mechanical properties of electrospun PCL/PGA blend nanofibers. *J. Appl. Polym. Sci.* **2011**, *124*, 123–131. [[CrossRef](#)]
76. Fang, Y.; Zhu, X.; Wang, N.; Zhang, X.; Yang, D.; Nie, J.; Ma, G. Biodegradable core-shell electrospun nanofibers based on PLA and γ -PGA for wound healing. *Eur. Polym. J.* **2019**, *116*, 30–37. [[CrossRef](#)]
77. Villa, F.; Marengo, M.; De Coninck, J. A new model to predict the influence of surface temperature on contact angle. *Sci. Rep.* **2018**, *8*, 6549. [[CrossRef](#)]
78. Fowkes, F.M. Attractive forces at interfaces. *Ind. Eng. Chem.* **1964**, *56*, 40–52. [[CrossRef](#)]
79. Strnad, G.; Chirila, N.; Petrovan, C.; Russu, O. Contact Angle Measurement on Medical Implant Titanium Based Biomaterials. *Procedia Technol.* **2016**, *22*, 946–953. [[CrossRef](#)]
80. Xu, L.C.; Siedlecki, C.A. Effects of surface wettability and contact time on protein adhesion to biomaterial surfaces. *Biomaterials* **2007**, *28*, 3273–3283. [[CrossRef](#)] [[PubMed](#)]
81. Peponi, L.; Navarro-Baena, I.; Báez, J.E.; Kenny, J.M.; Marcos-Fernández, A. Effect of the molecular weight on the crystallinity of PCL-b-PLLA di-block copolymers. *Polymer* **2012**, *53*, 4561–4568. [[CrossRef](#)]
82. Olubamiji, A.D.; Izadifar, Z.; Si, J.L.; Cooper, D.M.; Eames, B.F.; Chen, D.X. Modulating mechanical behaviour of 3D-printed cartilage-mimetic PCL scaffolds: Influence of molecular weight and pore geometry. *Biofabrication* **2016**, *8*, 025020. [[CrossRef](#)] [[PubMed](#)]
83. Perstorp. CAPA 6000 Series Datasheet. Available online: <http://www.rapstrap.com/TDS-CAPA6500.pdf> (accessed on 11 August 2022).
84. Liu, H.; Webster, T.J. Bioinspired nanocomposites for orthopedic applications. In *Nanotechnology for the Regeneration of Hard and Soft Tissues*; World Scientific: Singapore, 2007; pp. 1–51. ISBN 978-981-270-615-7.
85. Doyle, S.E.; Henry, L.; McGennisken, E.; Onofrillo, C.; Bella, C.D.; Duchi, S.; O’Connell, C.D.; Pirogova, E. Characterization of Polycaprolactone Nanohydroxyapatite Composites with Tunable Degradability Suitable for Indirect Printing. *Polymers* **2021**, *13*, 295. [[CrossRef](#)] [[PubMed](#)]
86. Germiniani, L.G.L.; da Silva, L.C.E.; Plivelic, T.S.; Gonçalves, M.C. Poly(ϵ -caprolactone)/cellulose nanocrystal nanocomposite mechanical reinforcement and morphology: The role of nanocrystal pre-dispersion. *J. Mater. Sci.* **2018**, *54*, 414–426. [[CrossRef](#)]
87. Chiu, Y.C.; Fang, H.Y.; Hsu, T.T.; Lin, C.Y.; Shie, M.Y. The Characteristics of Mineral Trioxide Aggregate/Polycaprolactone 3-dimensional Scaffold with Osteogenesis Properties for Tissue Regeneration. *J. Endod.* **2017**, *43*, 923–929. [[CrossRef](#)]
88. Bellani, C.F.; Pollet, E.; Hebraud, A.; Pereira, F.V.; Schlatter, G.; Avérous, L.; Bretas, R.E.S.; Branciforti, M.C. Morphological, thermal, and mechanical properties of poly(ϵ -caprolactone)/poly(ϵ -caprolactone)-grafted-cellulose nanocrystals mats produced by electrospinning. *J. Appl. Polym. Sci.* **2016**, *133*. [[CrossRef](#)]
89. Gagol, M.; Soltani, R.D.C.; Przyjazny, A.; Boczka, G. Effective degradation of sulfide ions and organic sulfides in cavitation-based advanced oxidation processes (AOPs). *Ultrason. Sonochemistry* **2019**, *58*, 104610. [[CrossRef](#)]
90. Giannoudis, P.V.; Pountos, I. Tissue regeneration: The past, the present and the future. *Injury* **2005**, *36*, S2–S5. [[CrossRef](#)] [[PubMed](#)]
91. Forbes, S.J.; Rosenthal, N. Preparing the ground for tissue regeneration: From mechanism to therapy. *Nat. Med.* **2014**, *20*, 857–869. [[CrossRef](#)] [[PubMed](#)]

Disclaimer/Publisher’s Note: The statements, opinions and data contained in all publications are solely those of the individual author(s) and contributor(s) and not of MDPI and/or the editor(s). MDPI and/or the editor(s) disclaim responsibility for any injury to people or property resulting from any ideas, methods, instructions or products referred to in the content.